High Power Laser Science and Engineering, (2023), Vol. 11, e87, 6 pages.
doi:10.1017/hpl.2023.73

HIGH POWER LASER SCIENCE AND ENGINEERING

RESEARCH ARTICLE

Demonstration of a diode-pumped dual-wavelength metastable krypton laser

Qingshan Liu[1,2,3,†], Rui Wang[1,2,3,†], Zining Yang[1,2,3], Jianyong Sun[1,2], Weiqiang Yang[1,2,3], Hongyan Wang[1,2,3], and Xiaojun Xu[1,2,3]

[1] *College of Advanced Interdisciplinary Studies, National University of Defense Technology, Changsha, China*

[2] *Nanhu Laser Laboratory, National University of Defense Technology, Changsha, China*

[3] *Hunan Provincial Key Laboratory of High Energy Laser Technology, National University of Defense Technology, Changsha, China*

(Received 19 June 2023; revised 13 August 2023; accepted 7 September 2023)

Abstract

Diode-pumped rare gas lasers are potential candidates for high-energy and high-beam quality laser systems. Currently, most investigations are focused on metastable Ar lasers. The Kr system has the unique advantages of higher quantum efficiency and lower discharge requirements for comparison. In this paper, a diode-pumped metastable Kr laser was demonstrated for the first time. Using a repetitively pulsed discharge at a Kr/He pressure of up to approximately 1500 Torr, metastable Kr atoms of more than 10^{13} cm^{-3} were generated. Under diode pumping, the laser realized a dual-wavelength output with an average output power of approximately 100 mW and an optical conversion efficiency of approximately 10% with respect to the absorbed pump power. A kinetics study involving population distribution and evolution was conducted to analyze the laser performance.

Keywords: diode pump; krypton; metastable rare gas laser

1. Introduction

Currently, extensive research has shown that diode-pumped metastable rare gas lasers (DPRGLs) have the potential for high-power laser output with excellent beam quality[1–11]. Han and Heaven[1] first proposed the laser concept in 2012, in which the gain and lasing were demonstrated. DPRGLs use metastable rare gas atoms (Rg* represents the metastable rare gas atoms Ar*, Kr* and Xe*) excited through electron collisions as the laser gain medium. Due to the similarity of the electronic configuration and optical property between the metastable rare gas atom and the alkali atom, DPRGLs are expected to inherit the single-aperture power-scaling potential of diode-pumped alkali vapor lasers (DPALs)[3,12,13]. In addition, using rare gas as the laser medium is convenient and safe for high-power laser systems.

DPRGLs are usually expected to operate in a three-level system, as illustrated in Figure 1. The energy levels represented by Paschen and Racah notation are displayed, which takes Kr as an example. In the laser cycle, the atom at $1s_5$ (Kr*) is preliminarily produced by electron collisions. Then the atom is excited to $2p_9$ by the diode pumping light and then relaxed to $2p_{10}$ through the collisional process by helium. The laser occurs through the stimulated emission transition from $2p_{10}$ to $1s_5$.

After a proof-of-concept demonstration of the laser using an optical parametric oscillator as a surrogate pump source in 2012, the first diode-pumped Ar* laser was realized in 2013[14]. Subsequently, Rawlins *et al.*[4] achieved a highly efficient continuous-wave Ar* laser with an apparent optical conversion efficiency of 55%. The research of Han *et al.*[2] revealed that persistent, high-density and large-volume generation of metastable laser could be obtained using a high-repetition nanosecond pulsed direct current (DC) discharge, and a continuous-wave Ar* DPRGL was realized with 4 W output. Eshel and Perram[3] established an advanced model to evaluate the scaling potential of DPRGLs, which theoretically demonstrated the feasibility of a highly efficient 100 kW-level Ar* laser. Wang *et al.*[8,9] recently proposed a new scheme for extracting lasing in a plasma jet, potentially overcoming the power-scaling obstacles in previously used confined discharges.

Correspondence to: Zining Yang, College of Advanced Interdisciplinary Studies, National University of Defense Technology, Changsha 410073, China. Email: yangzining09@nudt.edu.cn

[†]These authors contributed equally to this work.

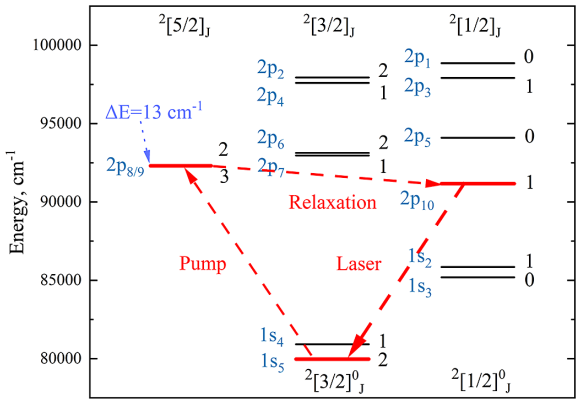

Figure 1. Energy levels and transition process of Kr (1s and 2p).

Until now, most research on DPRGLs has been carried out using Ar* as the gain medium[15–18] and a little on the Xe* laser[5,19,20]. The only research for the Kr* laser is on concept verification and kinetics investigation[1,21], and no study using high-power diode pumping has been reported. As compared with Ar*, Kr* has some noteworthy characteristics. Firstly, Kr* has lower excitation energy (Kr*: 9.92 eV versus Ar*: 11.55 eV), which could reduce the requirement for gas discharge and is beneficial to generate high-density metastables. Secondly, the quantum efficiency of Kr* is higher (Kr: 91% versus Ar: 89%), meaning a better optical conversion efficiency and less waste heat. Thirdly, the energy difference between the $2p_8$ and $2p_9$ levels of Kr is only 13 cm^{-1}, which means that a significant fraction of the population will locate among the three upper levels ($2p_8$, $2p_9$ and $2p_{10}$), creating conditions suitable for multi-wavelength laser emission.

In this work, we aim to explore the performance of a diode-pumped Kr* laser. The Kr* was generated using a repetitive nanosecond pulsed DC discharge. Under 811.3 nm diode pumping, a Kr* laser with dual wavelengths was demonstrated. The population distribution in the 2p levels and population time evolution in the 1s levels were monitored and analyzed to understand the laser kinetics further.

2. Experimental setup

The main experiment setup of the diode-pumped Kr* laser is shown in Figure 2. The gas discharge chamber was made of poly-ether-ether-ketone (PEEK) plastic with optical windows installed around four surfaces. Two circular plane electrodes (tungsten copper alloy) were mounted face-to-face in the chamber's center. They had a cross-section of $\pi \times 2.5^2$ mm^2 and were separated by a distance of 3 mm. A dry scroll vacuum pump (IDP-15, Agilent Technologies) was used to evacuate impurified gas from the chamber in advance. The mixed Kr:He gas (1:49 and 99.999% in purity) was fed into the gas chamber. A mass flow meter was used to control the flow rate at 2 L/min, and a choke valve was used to adjust the pressure inside the chamber.

The plasma was produced by gas discharge using a nanosecond pulsed DC power source, which could run at a voltage of approximately 4 kV, a pulse duration of 80 ns and a maximum frequency of 200 kHz. When the pulsed DC power supply was turned on, the generated plasma could fill the whole space between the two electrodes. The discharge voltage between the two electrodes was measured by a high-voltage differential probe (P6015A, Tektronix).

In Figure 2, a longitudinal pump scheme was used to excite the Kr* laser. The wavelength of the diode pumping source was locked by a volume-Bragg grating at the central wavelength ($1s_5 \rightarrow 2p_9$) of 811.29 nm, and the pump source could produce approximately 7.6 W output power with a linewidth of 0.1 nm (full width at half maximum (FWHM)). The measured absorption bandwidth of the pump transition was 0.029 nm (FWHM) at the pressure of 600 Torr and

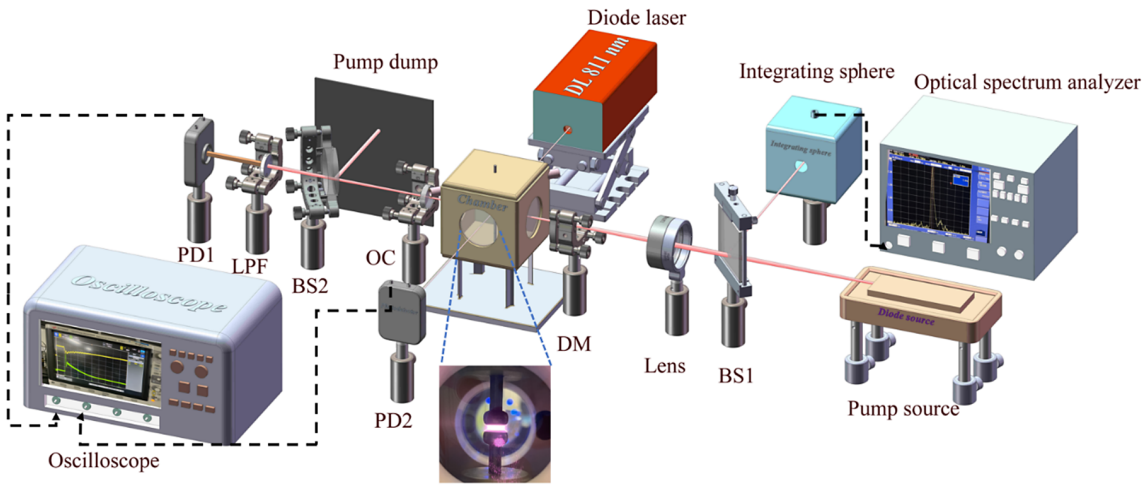

Figure 2. Schematics of the experimental setup of a diode-pumped Kr* laser. BS, beam splitter; DM, dichroic mirror; OC, output coupler; LPF, long pass filter; PD, photodetector.

0.062 nm at the pressure of 1450 Torr. The absorption bandwidth has an approximately linear change with the increasing mixed gas pressure (Kr:He = 1:49). A beam splitter (BS1) placed in front of the pump source could reflect approximately 5% of the pump light into an integrating sphere connected to an optical spectrum analyzer (OSA, AQ6370D, Yokogawa) for wavelength monitoring. A convex lens (lens, f = 150 mm) was used to focus the pump light into the central region of the plasma. The resonator with a length of approximately 160 mm consisted of a plane dichroic mirror (DM) and an output coupler (OC). The DM has more than 95% reflectivity at 892/877 nm and more than 95% transmittance at 811 nm. The OC is a concave mirror (500 mm radius of curvature) with approximately 90% reflectivity at 892 nm, approximately 80% reflectivity at 877 nm and more than 99% transmittance at 811 nm. To separate the Kr* laser from the pump light, a beam splitter (BS2, ~20% transmittance at 892 nm, ~5% transmittance at 877 nm and >99% reflectivity at 811 nm) was used to reflect most of the transmitted pump light into a pump dump, and a long pass filter (LPF, Thorlabs, cut at the wavelength 850 nm) was used to further filter out the residual pump light. A photodetector (PD1, DET10A2, Thorlabs) was used to collect the signal of the Kr* laser.

The atomic density measurement device was placed perpendicular to the pump path. The single-frequency probe laser (DL, UniQuanta, Inc.) has an approximately 1 MHz linewidth and a wide tuning range of more than 1 nm. It was used to scan the absorption spectrum of the $1s_5 \rightarrow 2p_9$ transition. PD2 was used to measure the absorption signal of the probe light. After the absorption line shape was obtained, the absorption cross-section could be deduced and the number density of Kr* could be calculated using Beer–Lambert's law.

3. Experimental results

The discharge apparatus could produce Kr* with a number density higher than 10^{13} cm^{-3}, and the atomic density evolution is plotted in Figure 3. The pressure was increased from 496 to 1465 Torr while keeping the voltage at a constant value of approximately 3 kV. The peak atomic density increased with elevating pressure, partially due to the increased absolute amount of Kr. The time duration between the peak value and 1/e of the atomic density was used to represent the apparent lifetime of Kr*. It decreased from 5.1 μs (at 496 Torr) to 1.67 μs (at 1465 Torr), mainly due to the more frequent quenching collisions at higher pressure.

The spectrum of the Kr* laser is shown in Figure 4, which presents the dual laser lines of 877 nm ($2p_8 \rightarrow 1s_4$) and 892 nm ($2p_{10} \rightarrow 1s_5$). The 892 nm spectrum originated from the expected three-level cycle $1s_5 \rightarrow 2p_9 \rightarrow 2p_{10} \rightarrow 1s_5$, while the 877 nm spectrum originated from the additional channel $1s_5 \rightarrow 2p_9 \rightarrow 2p_8 \rightarrow 1s_4$. The energy gap between the $2p_8$ and

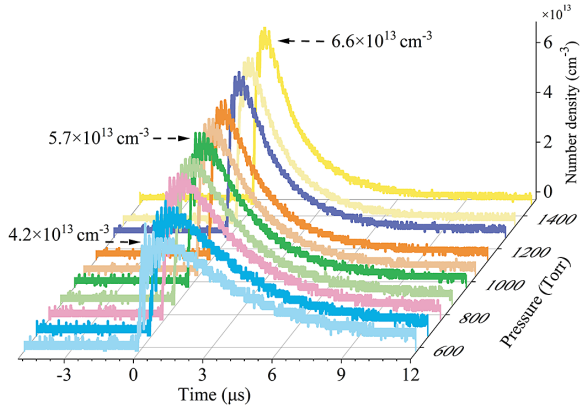

Figure 3. Time-dependent number density of Kr* at different pressures.

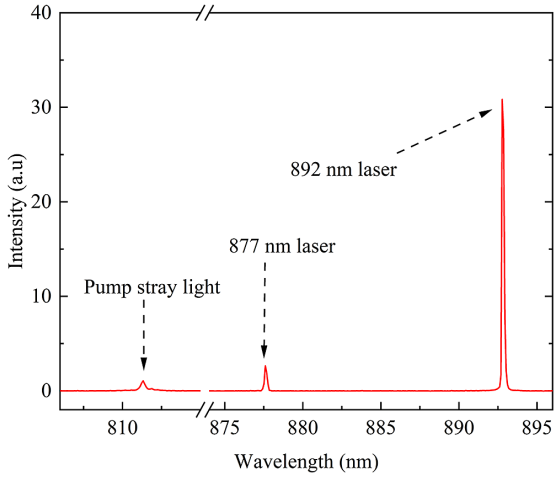

Figure 4. Spectrum of the output laser (877 and 892 nm) and the pump stray light (811 nm).

$2p_9$ levels is only 13 cm^{-1}. A kinetics study in Kr showed that the populations of $2p_8$ and $2p_9$ were in Boltzmann thermal equilibrium due to the fast collisional mixing rate at atmospheric helium[21]. So, a considerable amount of the population was transferred to the $2p_8$ state (~70% relative to $2p_9$), which supported the lasing due to population inversion between $2p_8$ and $1s_4$.

The time-dependent traces of the discharge voltage, the number density of $1s_5$ and the laser intensity are shown in Figure 5. The discharge operated at a voltage of approximately 3.6 kV with a frequency of 200 kHz. After each discharge pulse, the number density of $1s_5$ reached a peak value of approximately 5.5×10^{13} cm^{-3} and decreased to 1×10^{13} cm^{-3} within 5 μs under the pressure of 1125 Torr. When the pump was on, pulsed Kr* lasing was observed, with an initial spike and a decreased trend similar to the atomic density evolution.

The averaged power of the Kr* laser is shown in Figure 6. The laser power increased linearly with pressure, which may arise from the increased number density of Kr* and faster

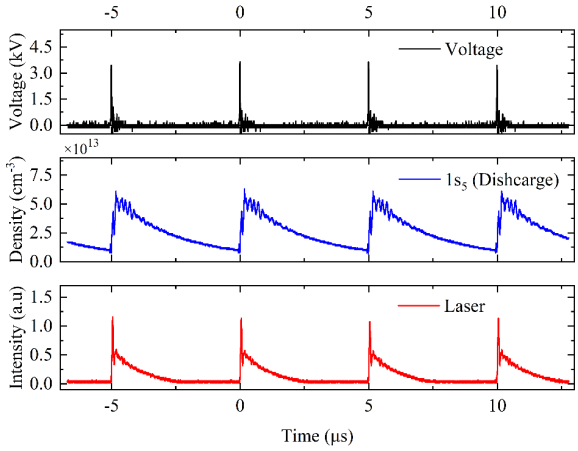

Figure 5. Time-dependent traces for the voltage between two electrodes, the number density of Kr ($1s_5$) under discharge only and the laser intensity under 7.6 W pump power.

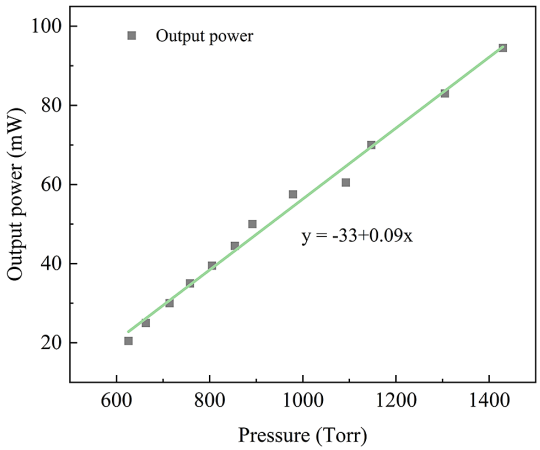

Figure 6. Laser power of the Kr* laser with increasing pressure, under 7.6 W pump power.

collisional relaxation from $2p_9$ to the upper laser levels. At the pressure of 1430 Torr, the maximum output power reached approximately 100 mW and the absorbed pump power was approximately 1 W, which meant that the optical conversion efficiency was approximately 10%. The peak power calculated from the lasing trace was approximately 1.1 W.

4. Discussion

The dual-wavelength Kr* laser was achieved with an optical conversion efficiency of approximately 10%. To investigate the muti-wavelength mechanism and the low optical conversion efficiency, the methods of optical emission spectroscopy (OES) and tunable diode laser absorption spectroscopy (TDLAS) were employed to study the population distribution and evolution of the populations in this Kr* laser.

4.1. Population distribution of the 2p energy levels

The line-ratio method of OES used to obtain the Rg (2p) population distribution was described in detail in our previous work[22]. Transitions from the 2p states with strong emission intensity were chosen to reveal the 2p populations due to their high signal-to-noise ratio. The population distribution of the total 2p levels at pressure of approximately 1100 Torr is presented in Figure 7(a). When only discharge existed ('discharge only'), a small number of atoms occupied the 2p levels. When the diode pump light entered the medium with no lasing ('pumping without a resonator'), a significant increase in population at energy levels of $2p_8$, $2p_9$ and $2p_{10}$ was observed. In addition, some excited atoms relaxed to adjacent energy levels of $2p_6$ and $2p_7$, while a few atoms were transferred to higher levels ($2p_1$ to $2p_5$). When the resonator was established with lasing ('pumping with lasing'), approximately 4.5% of the atoms in the $2p_{10}$ level were consumed due to stimulated radiation. In addition, the increase in population at the $2p_8$ and $2p_9$ levels was caused by the enhanced pump absorption in the laser cycle, resulting in more Kr* being pumped to the $2p_9$ level and simultaneously relaxed to the $2p_8$ level. The population distribution suggested that the observed dual-wavelength emission was attributed to a significant proportion of atoms populated in the $2p_8$ and $2p_{10}$ levels.

To investigate the relationship between power and pressure (Figure 6), the population ($2p_8$–$2p_{10}$) in the condition of 'pumping with lasing' was studied with a wide range of pressure, plotted in Figure 7(b). The proportion of populations in $2p_1$–$2p_7$ was small (~10% at a pressure of 400 Torr, ~1% at a pressure of 1400 Torr) and is not shown here. The population growth of $2p_{10}$ was significant with increasing pressure, whereas $2p_9$ exhibited weaker growth. Furthermore, $2p_8$ also experienced increased growth under pressure until reaching a plateau at atmospheric pressure. Therefore, the observed increase in the output power can be ascribed to an increased upper laser level population.

4.2. Population evolution of the 1s energy levels

Similar to Ar[14,23], for the 1s manifold of Kr, the $1s_4$ and $1s_5$ levels are the primary influencing levels. To reveal the kinetics of $1s_4$ and $1s_5$, two probe lasers with wavelengths of 819 nm ($1s_4 \rightarrow 2p_6$) and 811.3 nm ($1s_5 \rightarrow 2p_9$) were used to monitor the absorption signal of the $1s_4$ and $1s_5$ levels simultaneously. The population evolutions are shown in Figure 8. With discharge only, a certain number of atoms were excited to the $1s_4$ and $1s_5$ levels. When the pump was on, the number density of $1s_5$ decreased, while that of the $1s_4$ increased. The accumulation in the $1s_4$ level mainly arose from the spontaneous radiation of the $2p_8$ and $2p_{10}$ levels. Considering the spontaneous emission coefficients and the populations of the two levels (Figure 7), the contributions

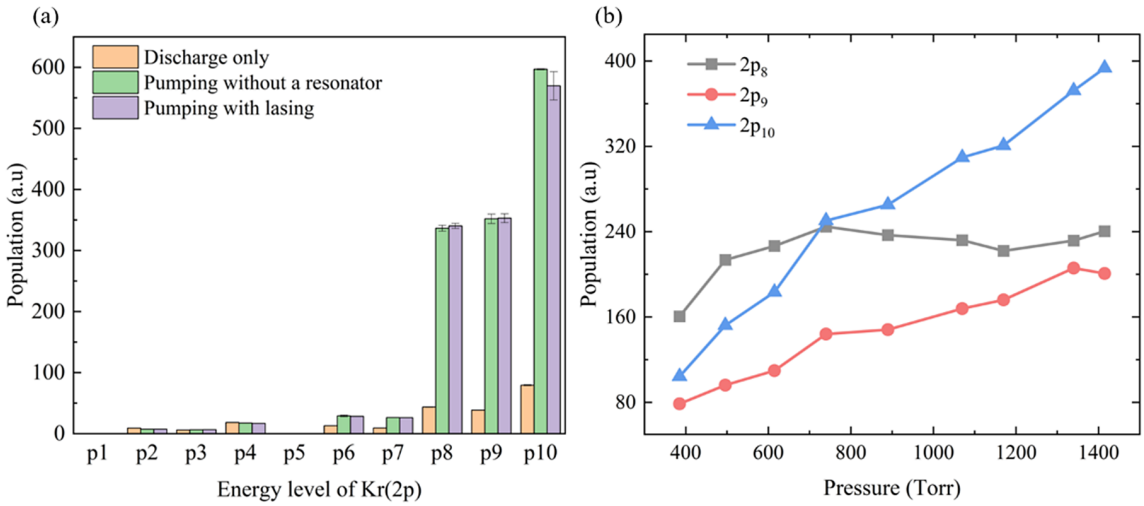

Figure 7. (a) Population distribution in Kr (2p) (the error bar represents standard deviation) and (b) population of Kr ($2p_8$, $2p_9$ and $2p_{10}$) versus pressure.

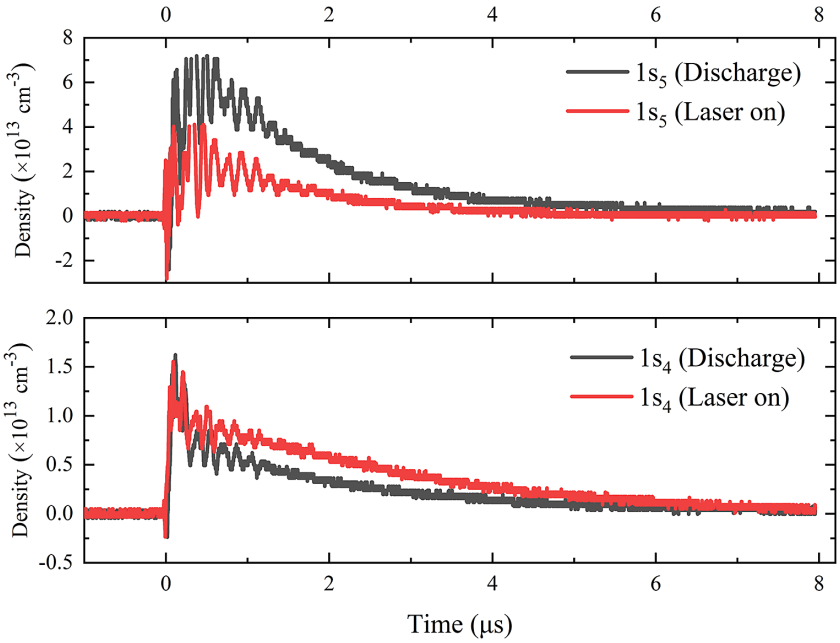

Figure 8. Time-dependent traces of the number density of the $1s_5$ and $1s_4$ levels. (The oscillation in the figure is the noise of the discharge.)

that repopulated $1s_4$ were nearly 3.8:1 for $2p_8$ and $2p_{10}$. The time-dependent trace of $1s_4$ also showed that the atomic relaxation from $1s_4$ to $1s_5$ was slower than the spontaneous radiation. These factors caused the depletion of Kr* and the early termination of the laser. The accumulation of $1s_4$ could be significantly improved by increasing the $1s_5$ density and using a dual-wavelength pump scheme[6,7].

5. Conclusion

In conclusion, a dual-wavelength diode-pumped metastable Kr laser was demonstrated for the first time. The high number density of Kr* ($>10^{13}$ cm^{-3}) was obtained in a wide pressure range in the pulsed DC discharge. The dual wavelengths of 877 and 892 nm with an averaged power of approximately 100 mW (peak power ~1.1 W) and an apparent optical conversion efficiency of approximately 10% with respect to the absorbed pump power were achieved. In order to explain the dual-wavelength phenomenon and the low efficiency, the population distribution of the 2p levels was revealed using the OES method, and the population evolution of the 1s levels was monitored using the TDLAS method. The dual-wavelength output mainly arose from the large population in the $2p_8$ and $2p_{10}$ levels. The low efficiency was caused by several improvable reasons, including insufficient column density of Kr*, low pump intensity, the accumulation in $1s_4$, etc.

In the next step, conditions should be synthetically optimized to validate the high-power and high-efficiency potential of the Kr* laser. Firstly, compared with Ar*, Kr* could sustain a stable discharge and larger volume under higher pressure, and a higher column density may be obtained by optimizing the discharge parameters. Secondly, the currently available pump intensity (~0.5 kW/cm^2) was far below the requirement, approximately near the threshold. The diode pump source power and intensity will be improved. Thirdly, an increase in the metastable density and the dual-wavelength pumping scheme is expected to eliminate the accumulation effect of $1s_4$.

References

1. J. Han and M. C. Heaven, Opt. Lett. **37**, 2157 (2012).
2. J. Han, M. C. Heaven, P. J. Moran, G. A. Pitz, E. M. Guild, C. R. Sanderson, and B. Hokr, Opt. Lett. **42**, 4627 (2017).
3. B. Eshel and G. P. Perram, J. Opt. Soc. Am. B **35**, 164 (2018).
4. W. T. Rawlins, K. L. Galbally-Kinney, S. J. Davis, A. R. Hoskinson, J. A. Hopwood, and M. C. Heaven, Opt. Express **23**, 4804 (2015).
5. C. R. Sanderson, C. W. Ballmann, J. Han, A. B. Clark, B. H. Hokr, K. G. Xu, and M. C. Heaven, Opt. Express **27**, 36011 (2019).
6. P. Sun, D. Zuo, X. Wang, J. Han, and M. C. Heaven, Opt. Express **28**, 14580 (2020).
7. Z. Yang, G. Yu, H. Wang, Q. Lu, and X. Xu, Opt. Express **23**, 13823 (2015).
8. R. Wang, Z. Yang, Q. Liu, K. Han, H. Wang, and X. Xu, Opt. Lett. **47**, 3279 (2022).
9. X. Xu, R. Wang, and Z. Yang, Opto-Electron. Adv. **6**, 220113 (2023).
10. P. A. Mikheyev, Quantum Electron. **45**, 704 (2015).
11. A. V. Demyanov, I. V. Kochetov, and P. A. Mikheyev, J. Phys. D **46**, 375202 (2013).
12. J. Zweiback, A. Komashko, and W. F. Krupke, Proc. SPIE **7581**, 75810G (2010).
13. W. F. Krupke, Prog. Quantum Electron. **36**, 4 (2012).
14. J. Han, L. Glebov, G. Venus, and M. C. Heaven, Opt. Lett. **38**, 5458 (2013).
15. D. J. Emmons, D. E. Weeks, B. Eshel, and G. P. Perram, J. Appl. Phys. **123**, 043304 (2018).
16. P. A. Mikheyev, A. K. Chernyshov, M. I. Svistun, N. I. Ufimtsev, O. S. Kartamysheva, M. C. Heaven, and V. N. Azyazov, Opt. Express **27**, 38759 (2019).
17. W. T. Rawlins, A. R. Hoskinson, K. L. Galbally-Kinney, S. J. Davis, J. A. Hopwood, J. Han, and M. C. Heaven, J. Phys. Chem. A **127**, 2489 (2023).
18. A. R. Hoskinson, J. Gregorío, J. Hopwood, K. Galbally-Kinney, S. J. Davis, and W. T. Rawlins, J. Appl. Phys. **119**, 233301 (2016).
19. P. A. Mikheyev, J. Han, A. Clark, C. Sanderson, and M. C. Heaven, J. Phys. D **50**, 485203 (2017).
20. A. V. Demyanov, I. V. Kochetov, P. A. Mikheyev, V. N. Azyazov, and M. C. Heaven, J. Phys. D **51**, 045201 (2018).
21. J. Han and M. C. Heaven, Opt. Lett. **40**, 1310 (2015).
22. Q. Liu, R. Wang, J. Sun, H. Zhao, Z. Yang, W. Yang, H. Wang, K. Han, and X. Xu, Opt. Express **31**, 22092 (2023).
23. R. Wang, Q. Liu, Z. Yang, H. Wang, and X. Xu, Opt. Lett. **47**, 5477 (2022).